Int J Thermophys (2007) 31:1945–1951
DOI 10.1007/s10765-008-0516-8

Diffusive-Ballistic Heat Conduction of Carbon Nanotubes and Nanographene Ribbons

Junichiro Shiomi · Shigeo Maruyama

Published online: 16 October 2008

Abstract Investigations of diffusive-ballistic heat conduction of finite-length single-walled carbon nanotubes and nanographene ribbons at room temperature have been carried out by using non-equilibrium molecular dynamics simulations. The length dependences of the thermal conductivity reveal the variation of the balance between ballistic and diffusive heat conductions. For both systems, the profile indicates a significant contribution of the ballistic phonon transport even with a length of about a micrometer. Comparison of the length effects of single-walled carbon nanotubes and nanographene ribbons highlights the roles of phonon dispersions and the extent of phonon scattering on diffusive-ballistic heat conduction.

Keywords Carbon nanotube · Nanographene ribbon · Thermal conductivity · Molecular dynamics

1 Introduction

Single-walled carbon nanotubes (SWNTs) are expected to play an important role in nanotechnology with diverse prospective applications including various electrical and thermal devices utilizing their unique electrical and thermal properties [1]. For actual applications of SWNTs, one of the essential tasks is to characterize their thermal

J. Shiomi (✉)
Department of Mechanical Engineering, The University of Tokyo, #62A3, Engineering Building II, 7-3-1 Hongo, Bunkyo-ku, Tokyo 113-8656, Japan
e-mail: shiomi@photon.t.u-tokyo.ac.jp

S. Maruyama
Department of Mechanical Engineering, The University of Tokyo, #63D4, Engineering Building II, 7-3-1 Hongo, Bunkyo-ku, Tokyo 113-8656, Japan
e-mail: maruyama@photon.t.u-tokyo.ac.jp

properties not only for thermal devices but also for electrical devices since they determine the affordable amount of electrical current through the system. With advances in SWNT synthesis and MEMS (microelectromechanical systems) techniques, thermal conductivity measurements of individual SWNTs and multi-wall carbon nanotubes have been recently reported [2–6]. However, the experimental measurements of SWNT thermal properties are still extremely challenging, and there is a great demand for reliable theories and numerical simulations, especially for investigations of detailed heat-transfer characteristics that are not accessible in experiments.

The phonon mean free path of an SWNT is expected to be extraordinarily long due to the strong carbon bonds and quasi-one-dimensional confinement of phonons. Consequently, the ballistic phonon transport regime stretches beyond the realistic length in many applications even at room temperature. At room temperature, since a considerable range of phonon branches are populated, the phonon relaxation time strongly varies among different phonons; thus, the phonon transport is expected to exhibit complex diffusive-ballistic features. This gives rise to some unique stationary and non-stationary heat conduction [7,8]. One of the most important consequences of diffusive-ballistic phonon transport in practical situations is the dependence of the thermal conductivity on the geometry (length and diameter) of SWNTs [9–13]. In this paper, by using non-equilibrium molecular dynamics (MD) simulations, we characterize diffusive-ballistic heat conduction of SWNTs and its geometry dependence. The geometrical effect on the diffusive-ballistic heat conduction is explored by investigating the heat conduction of a finite-length nanographene ribbon (NGR). We consider an artificial NGR with periodic boundary conditions in the spanwise direction, i.e., an unfolded SWNT maintaining circumferential periodicity (Fig. 1). The NGR possesses the same number of atoms per unit cell as the corresponding SWNT but exhibits different eigenstates due to the curvature relaxation. The strategy is to solely investigate the curvature effect on the heat conduction by carrying out comparisons without complications caused by the localized phonon states and boundary phonon scattering at the edge of a graphene of finite width [14,15].

2 Molecular Dynamics Simulations

The carbon–carbon interactions were modeled by adopting the Brenner potential [16] in a simplified form [17]. The potential model can describe a variety of small hydrocarbons, graphite, and diamond lattices. The basic formulation of the potential is based on the covalent-bonding treatment developed by Tersoff [18]. The total potential energy of the system E_b is expressed as the sum of the bonding energy of each bond between carbon atoms i and j:

$$E_b = \sum_i \sum_{j(i<j)} \left[V_R(r_{ij}) - B^*_{ij} V_A(r_{ij}) \right]. \tag{1}$$

Here, $V_R(r)$ and $V_A(r)$ are the repulsive and attractive force terms, which take a Morse-type form with a certain cutoff function. B^*_{ij} represents the effect of the bonding order parameters. We chose the potential parameters that have been shown to reproduce force

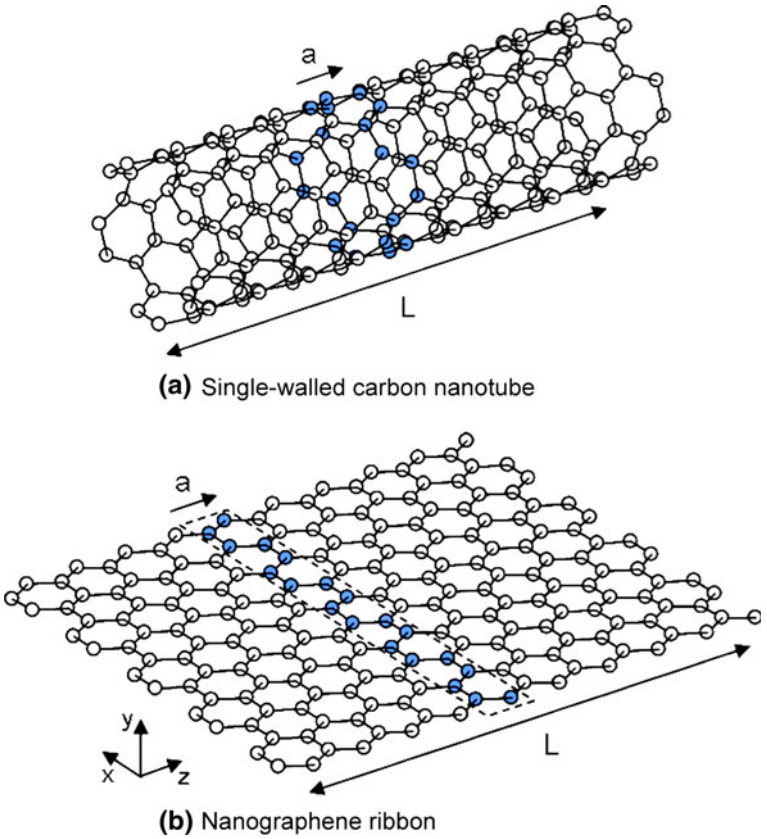

Fig. 1 Sketches of (**a**) a (5,5)-SWNT and (**b**) corresponding (5,5)-NGR with length L. Solid atoms indicate the unit cells. Vector 'a' denotes the translation vector. A period boundary condition is applied in the x-direction for the NGR, which is essentially an unfolded SWNT

constants with sufficient accuracy [9,10]. The velocity Verlet method was adopted to integrate the equation of motion with a time step of 0.5 fs. The dispersion relations of the system can be visualized using MD simulations by taking the two-dimensional Fourier spectra of the time history of the one-dimensional velocity field along a system. The periodic boundary condition was applied in the longitudinal (z) direction (Fig. 1). The phonon energy spectral density is computed as

$$\Phi(\omega, k) = \frac{m}{2} \sum_{\alpha}^{p} \sum^{3} \left| \frac{1}{N} \sum_{n=0}^{N-1} \left[\mathrm{e}^{i \frac{n}{N} k} \int v_\alpha(n, t) \mathrm{e}^{-i\omega t} \mathrm{d}t \right] \right|^2, \quad (\alpha = x, y, z), \quad (2)$$

where N is the number of atoms in the longitudinal (z) direction. Here, p and m are the number of atoms per unit cell and the mass of a carbon atom, respectively. In Fig. 2, the spectra of a 12.5 nm (5,5)-SWNT and the corresponding NGR at 300 K are presented. The data are discrete due to the finite system length, and the broadening of the

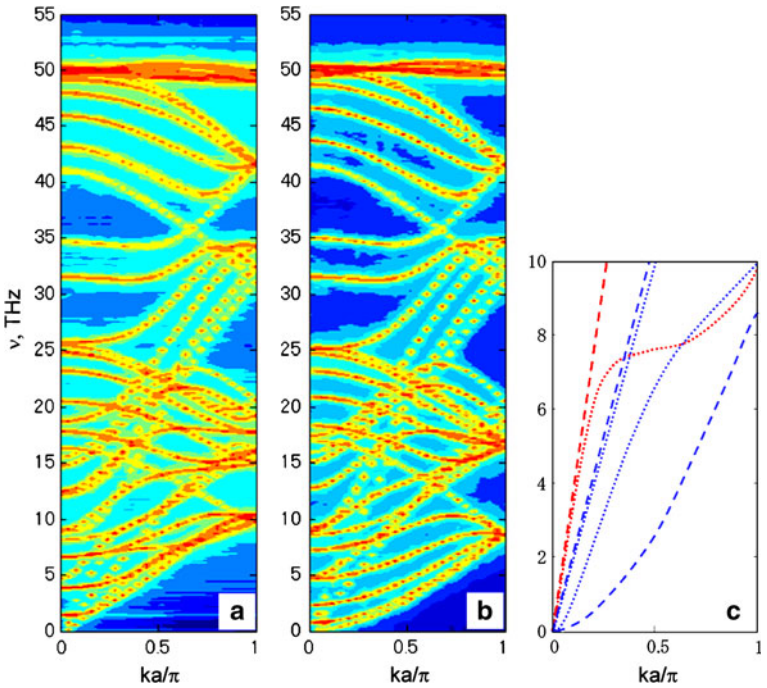

Fig. 2 Discrete phonon dispersions of (**a**) a 12.5-nm long (5,5)-SWNT and (**b**) NGR. The dispersion relations were visualized by computing the energy density spectra from MD simulations. Sketch of the low frequency regime (**c**) denotes the dispersions of acoustic phonon branches for the SWNT (*dotted line*) and NGR (*dashed line*). Red and blue denote longitudinal and transverse phonons, respectively (Colored online)

spectral peaks indicates the extent of thermal phonon scattering. The overall feature of dispersion relations of SWNT obtained from MD simulations agrees with reported theoretical models [1,19], especially with the model of Mahan and Jeon [19]. As seen in Fig. 2, while the dispersion relations of the (5,5)-SWNT and (5,5)-NGR exhibit similar overall zone-folded features, the difference is evident especially for lower frequency phonons, which in general are considered to be the primary heat carrier. It can be observed in the low-frequency regime that the unfolding bends the branches toward lower frequency, which is mainly attributed to the relatively soft out-of-plane transverse modes of the NGR decoupled from in-plane modes.

The thermal conductivity λ of SWNTs and NGRs was calculated by using non-equilibrium MD simulations. After reaching an isothermal state at 300 K with the auxiliary velocity scaling control, the temperature-controlled layers on both ends of the system were activated to apply a temperature difference of 20 K. Eventually, the system converges to a quasi-stationary state with a linear temperature gradient. The simulation time varies within the range of (3 to 18) ns as the convergence time depends on the system size. By calculating the heat flux Q along the system from the energy budgets of the thermostats, λ was calculated using Fourier's law, $Q/A = -\lambda(\partial T/\partial z)$. The cross-sectional area A of an SWNT was defined using the ring of a van der Waals thickness πbd, where d is the nanotube diameter and $b = 0.34$ nm. We use the same

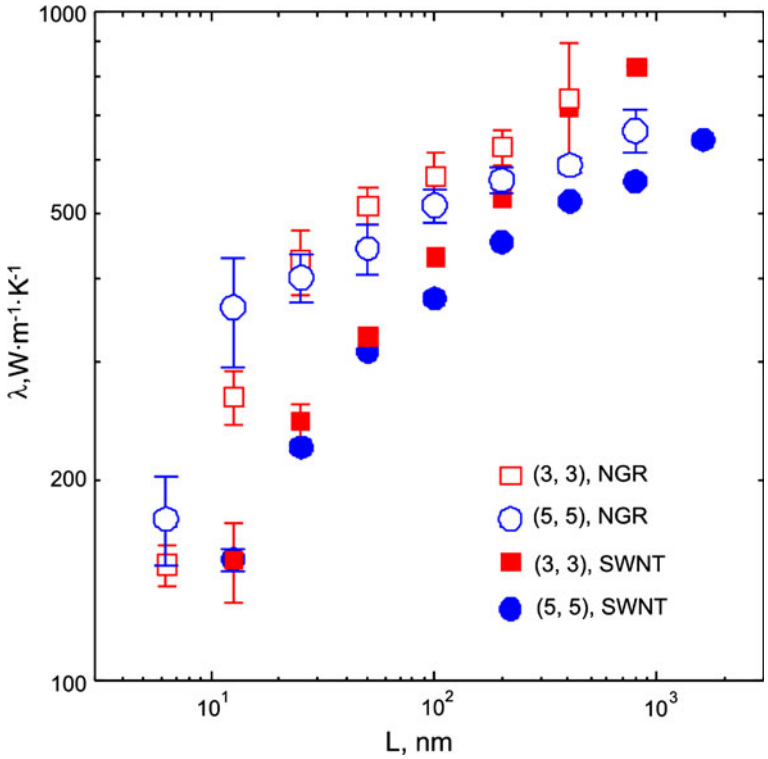

Fig. 3 Length dependences of the thermal conductivity of SWNTs and NGRs. Simulations were performed for two different chiral indices (3,3) and (5,5)

definition of A for NGRs to match the length scales for comparison with SWNTs. The usage of thermal conductivity to express the heat conduction of the current systems is arguable due to the extensive ballistic heat transport. Although simply expressing the heat conduction with the thermal conductance may be more suitable, here we use the thermal conductivity for the sake of comparison with previous studies. The computation of thermal conductivity was performed for a range of system lengths (L).

A temperature gradient was applied using the phantom technique as in previous studies [9,10]. The values of the thermal conductivity of (5,5)-SWNTs calculated with the phantom technique have been validated by performing additional simulations with a standard application of Nose–Hoover thermostats [20,21]. In the course of the validation, the length and relaxation time of the Nose–Hoover thermostat were tuned to reduce the virtual thermal boundary resistance between the temperature-controlled part and the rest of the nanotubes [13].

3 Results and Discussion

Figure 3 shows the length effect on the thermal conductivity of SWNTs and NGRs for a range of L. Simulations were performed for two different unit cell sizes with chiral

indices of (3,3) and (5,5). For both systems, the thermal conductivity did not converge in a range of L up to about a micrometer. The length dependence of the gradient of the profile clearly indicates the variation of the balance between diffusive and ballistic heat conductions for both SWNTs and NGRs. The gradient in the small L regime suggests significant ballistic heat conduction contributed from broad phonon branches [13]. Note that when the heat conduction is purely ballistic, the thermal conductance is constant and, hence, λ is proportional to L. When L is small, on considering the significant phonon population over a wide range of phonon branches at room temperature, we expect contributions to the heat conduction not only from ballistic transport of long wave-length acoustic phonons but also from phonons with wider ranges of wavenumber and frequency including optical phonons with sufficient group velocity.

As seen in Fig. 3, although the thermal conductivity keeps increasing with L as the effective mean free paths of the ballistic phonons increase, the gradient of the profiles gradually decreases since the number of ballistic phonons decreases. This suggests that, as L increases, the distribution of effective phonon mean free paths becomes broader and the increment of thermal conductivity is caused by more limited phonons with relatively long mean free paths such as long wavelength phonons with low frequency.

The thermal-conductivity profiles of SWNTs and NGRs exhibit distinct differences reflecting the differences in diffusive-ballistic phonon transport properties. Figure 3 shows that the thermal conductivity of NGRs is significantly higher than that of SWNTs, and the difference decreases as L increases. Let us now picture the thermal conductivity as a summation of each phonon transport, $\sum C_i v_i l_i$, where C_i, v_i, and l_i are the heat capacity, group velocity, and mean free path of the ith phonon, respectively. The dispersion relations have direct influence on the linear phonon transport properties $C_i v_i$; however, their variation is not sufficient to cause the difference seen in Fig. 3 as demonstrated at the ballistic heat conduction limit [22]. Hence, the current results suggest that a significant contribution comes from the variation in mean free paths. As seen in Fig. 2, evidently at frequencies less than 10 THz, by unfolding an SWNT to form an NGR, transverse phonon branches are bent and shifted downward in the intermediate wavenumber regime. These NGR phonon branches correspond to the out-of-plane transverse modes and are softer than the transverse phonon modes of the SWNT. As a result, the NGR possesses more low frequency phonon states than the SWNT. In general, the mean free path of phonons in an acoustic branch increases as the frequency decreases, where the scaling depends on the scattering process and the extent of anharmonicity. Therefore, one could attribute the current results to the difference in mean free paths of SWNTs and NGRs originating from the difference in the phonon dispersion relations.

Figure 3 also shows that the difference between thermal conductivities of SWNTs and NGRs decrease with increasing L. This is consistent with the above discussion that the major heat carriers change from broad short-range phonons with sufficient group velocity to a fewer but longer-range phonons with a smaller wavenumber and frequency as L becomes larger. Figure 2c denotes that the difference between dispersion relations of the SWNT and NGR is smaller for long wavelength acoustic phonons. In addition, in the small wavenumber regime, the bending transverse acoustic modes have a small group velocity due to their flexure feature [19]. Therefore, the

thermal conductivity variation due to the unfolding is expected to become smaller as L increases.

4 Conclusions

Non-equilibrium MD simulations were conducted to investigate the heat conduction of SWNTs and NGRs at room temperature. The length effects on the thermal conductivity were quantified over a range of L. The gradual transition from strongly ballistic to diffusive-ballistic heat conduction was clearly observed. The thermal conductivity of NGRs exhibits a significant difference from that of corresponding SWNTs, reflecting the differences in phonon dispersion relations.

Acknowledgments This work is supported in part by Grants-in-Aid for Scientific Research #19206024, #19054003, #19051016, and #19860022.

References

1. R. Saito, G. Dresselhaus, M.S. Dresselhaus, *Physical Properties of Carbon Nanotubes* (Imperial College Press, London, 1998)
2. C. Yu, L. Shi, Z. Yao, D. Li, A. Majumdar, Nano Lett. **5**, 1842 (2006)
3. E. Pop, D. Mann, Q. Wang, K. Goodson, H. Dai, Nano Lett. **6**, 96 (2006)
4. P. Kim, L. Shi, A. Majumdar, P.L. McEuen, Phys. Rev. Lett. **87**, 215502 (2001)
5. M. Fujii, X. Zhang, H. Xie, H. Ago, K. Takahashi, T. Ikuta, H. Abe, T. Shimizu, Phys. Rev. Lett. **95**, 065502 (2005)
6. J. Hone, M.C. Llaguno, M.J. Biercuk, A.T. Johnson, B. Batlogg, Z. Benes, J.E. Fischer, Appl. Phys. A **74**, 339 (2002)
7. J. Shiomi, S. Maruyama, Phys. Rev. B **73**, 205420 (2006)
8. J. Shiomi, S. Maruyama, Phys. Rev. B **74**, 155401 (2006)
9. S. Maruyama, Physica B **323**, 193 (2002)
10. S. Maruyama, Micro. Therm. Eng. **7**, 41 (2003)
11. N. Mingo, D.A. Broido, Nano Lett. **5**, 1221 (2005)
12. J. Wang, J.-S. Wang, Appl. Phys. Lett. **88**, 111909 (2006)
13. J. Shiomi, S. Maruyama, Jpn. J. Appl. Phys. **47**, 2005 (2008)
14. M. Igami, M. Fujita, S. Mizuno, Appl. Surf. Sci. **130–132**, 870 (1998)
15. T. Yamamoto, K. Watanabe, K. Mii, Phys. Rev. B **70**, 245402 (2004)
16. D.W. Brenner, Phys. Rev. B **42**, 9458 (1990)
17. Y. Yamaguchi, S. Maruyama, Chem. Phys. Lett. **286**, 336 (1998)
18. J. Tersoff, Phys. Rev. Lett. **56**, 632 (1986)
19. G.D. Mahan, G.S. Jeon, Phys. Rev. B **70**, 075405 (2004)
20. S. Nose, J. Chem. Phys. **81**, 511 (1984)
21. W.G. Hoover, Phys. Rev. A **31**, 1695 (1985)
22. N. Mingo, D.A. Broido, Phys. Rev. Lett. **95**, 096105 (2005)